



# 1 Analysis of 3GM High Accuracy Accelerometer 2 data collected during JUICE Lunar Earth Gravity Assist

3  
4 Authors: De Filippis Umberto<sup>1\*</sup>, Cappuccio Paolo<sup>2</sup>, Di Benedetto Mauro<sup>1</sup>, di Stefano Ivan<sup>1</sup>, Durante  
5 Daniele<sup>1</sup>, Iess Luciano<sup>1</sup>

6  
7 <sup>1</sup>Sapienza University of Rome, 00184 Rome, Italy, umberto.defilippis@uniroma1.it

8 <sup>1</sup>Sapienza University of Rome, 00184 Rome, Italy

9 <sup>2</sup>Aurora Technology BV for ESA, European Space Agency, European Space Astronomy Centre  
10 (ESAC), Camino Bajo del Castillo s/n, Villanueva de la Canada, 28692, Madrid, Spain

## 11 12 13 Abstract

14 The Jupiter ICy moons Explorer (JUICE) mission, launched in April 2023 by the European Space  
15 Agency (ESA), is designed to investigate Jupiter and its largest icy moons, Ganymede, Callisto, and  
16 Europa, with a focus on assessing their potential habitability and investigating subsurface oceans.  
17 During its eight-year interplanetary cruise to the Jovian system, JUICE will perform several flybys,  
18 including the first-ever combined Lunar-Earth Gravity Assist (LEGA), which occurred in August 2024.  
19 The spacecraft is equipped with a High Accuracy Accelerometer (HAA) that is part of the Gravity and  
20 Geophysics of Jupiter and the Galilean Moons (3GM) radio science instrument. During LEGA  
21 operations, HAA collected two hours of scientific data centered across the Moon's closest approach.  
22 We present here a detailed analysis of the HAA calibrated measurements that show a strong  
23 agreement with predicted non-gravitational accelerations, including those related to spacecraft  
24 deformation caused by the Moon's gravity gradient and thermoelastic displacements of the solar  
25 arrays during penumbra transitions. Additionally, unexpected dynamic responses were observed,  
26 including structural vibrations excited by the movement of the steerable telescope of the  
27 Submillimeter Wave Instrument (SWI) and a distinct outgassing event detected shortly after crossing  
28 the lunar terminator. The outgassing, likely involving sublimated water ice on the spacecraft, resulted  
29 in a measurable velocity change of  $0.7 \pm 0.1$  mm/s along the -Z spacecraft axis and a consequent  
30 mass loss of a few grams. This direction coincides with the normal direction of the spacecraft's most  
31 exposed surface to the Moon illuminated surface. The JUICE orbital reconstruction derived from radio  
32 tracking data collected by the Deep Space Transponder (DST) confirmed a consistent velocity  
33 variation, supporting HAA findings. These in-flight observations are essential for instrument  
34 calibration, characterization of the spacecraft's dynamic environment, and refining operational  
35 strategies.

## 36 1 Introduction

37  
38 The Jupiter ICy moons Explorer (JUICE) is an ESA large class mission launched on April 14, 2023 [1]  
39 Grasset *et al.*, (2013). It represents a significant opportunity to explore the Jovian system using a  
40 state-of-the-art suite of instruments. Focusing on Jupiter and its three largest icy moons, Ganymede,  
41 Callisto, and Europa, the mission's primary objective is to investigate the moons' potential habitability  
42 and the likely presence of subsurface oceans, which may harbor conditions suitable for life.  
43



44 The 8-year interplanetary cruise includes 3 Earth flybys and 1 Venus flyby, crucial for a timely arrival  
45 at Jupiter. The first Earth encounter after the launch was a lunar-Earth gravity assist (LEGA), occurred  
46 on August 19-20, 2024, and being the first-ever double gravity assist of human history in space  
47 exploration. This critical maneuver was essential for redirecting JUICE towards Venus, where another  
48 gravity assist occurred in August 2025. Subsequent flybys of the Earth in 2026 and 2029 will further  
49 refine the spacecraft's path, ensuring it will reach Jupiter with the correct speed and direction. These  
50 flybys are not merely navigational aids but also opportunities for scientific observations. These data  
51 could indeed contribute to refine our understanding of these bodies and support the calibration of  
52 JUICE's instruments.

53

54 Upon arrival at Jupiter in July 2031, JUICE will start its detailed exploration of the Jovian system,  
55 culminating in an extended circular polar and low altitude orbit phase around Ganymede. This phase  
56 will provide unprecedented insights into the moons' geology, extent of the subsurface ocean, and  
57 potential habitability, significantly advancing our knowledge of the outer Solar System [2] Grasset et  
58 al., (2023).

59

60 The High Accuracy Accelerometer (HAA) is one of the instrument onboard JUICE and its main goal is  
61 to support the Gravity and Geophysics of Jupiter and the Galilean Moons (3GM) radio science  
62 experiment. The accelerometer data will be used within the orbit determination process as a direct  
63 measurement of the non-gravitational perturbations acting on the spacecraft, particularly those due  
64 to the propellant sloshing. From the very early stages of the mission, HAA data played a crucial role in  
65 monitoring the spacecraft's deployable components. Within the first six weeks following JUICE's  
66 launch, the Mission Operation Control (MOC) team successfully deployed solar panels, antennas,  
67 probes, and booms that had been folded and latched during launch. The data collected by HAA  
68 offered valuable insights into the spacecraft's dynamics and a monitoring of the deployment  
69 operations [3] De Filippis et al., (2024).

70

71 During LEGA operations, HAA was switched ON in observation mode and collected data for two hours  
72 across the Moon closest approach (CA), providing direct measurements of the spacecraft's dynamics  
73 response to the solar eclipse, Moon gravity gradient and additional non gravitational perturbations  
74 acting on the probe.

75

76 The paper is organized as follows. In the following two sections the 3GM experiment and the HAA  
77 instrument are described. The third section deals about the LEGA geometry and HAA operations  
78 timeline. In the same section are discussed the expected and unexpected signals detected by HAA  
79 along with the instrument data analysis and interpretation. The last section contains conclusions.

80

## 80 2 The 3GM experiment

81

82 The 3GM instrument suite is devoted to radio science experiments, whose goals can be grouped in  
83 two main areas: geodesy and geophysics for Callisto, Europa and Ganymede, and atmospheric  
84 science of Jupiter. Gravity experiments will be performed using the Ka band two-way coherent radio  
85 link, enabled by the Ka band Transponder (KaT). Thanks to this state-of-art instrument, developed by  
86 Thales Alenia Space Italy, two-way range and Doppler observables can achieve a precision,  
87 respectively, of 4 cm at 10 s integration time (depending of the available signal to noise ratio) and of 3  
88  $\mu\text{m/s}$  at 1000 s integration time [4] Cappuccio et al., (2018); [5] Cappuccio et al., (2020). The  
89 occultation experiments will use the onboard ultra stable oscillator (USO), built by AccuBeat, to



90 perform accurate one-way radio occultations. The USO can generate onboard a highly stable 57.5  
91 MHz reference signal with an Allan deviation of about  $1 - 2 \times 10^{-13}$  over a broad range of integration  
92 times [1–1000 s] [6] A. Shapira et al., (2016).

93  
94 A previous analysis has shown that thanks to the Callisto's flybys, 3GM experiment will be capable to  
95 determine its gravity field up to degree and order 7 and improve notably the accuracy on the  
96 determination of the love number  $k_2$  ( $\sigma_{k_2} \leq 0.06$ ). The two close encounters of JUICE with Europa will  
97 allow 3GM to improve the knowledge of the quadrupole gravity field and verify the hydrostatic  
98 equilibrium hypothesis at the level of 0.5% [7] Cappuccio et al., (2022) .

99 However, the main objective of the JUICE mission is to perform a full tomography of Ganymede,  
100 thanks to the combination of 3GM observations with other instruments data.

101 Previous simulations showed that the moon's gravity field can be confidently determined up to degree  
102 35–40, together with a detailed characterization of the rotational state and tides [8] , [9]; Cappuccio  
103 et al.,(2020); De Marchi et al., (2022).

104 Furthermore, three superior solar conjunctions occurring during the cruise phase provide  
105 opportunities for the 3GM radio science experiment to perform tests of general relativity [10] di  
106 Stefano et al., (2022).

107 These scientific goals can be reached only if a very accurate dynamical model is used for the  
108 numerical integration of the spacecraft trajectory. Given the spacecraft structure, previous  
109 simulations showed that accelerations due to sloshing within the fuel tanks could severely affect the  
110 expected radio science outcome [11] Cappuccio et al., (2018). For this reason, 3GM will also exploit  
111 data collected by the on-board High Accuracy Accelerometer (HAA) to calibrate non-gravitational  
112 perturbations.

113

### 114 3 The High Accuracy Accelerometer

115 The High Accuracy Accelerometer is the second spring mass accelerometer ever flown on an  
116 interplanetary spacecraft. The instrument is built on the heritage of the Italian Spring Accelerometer  
117 (ISA) which is currently flying on BepiColombo ESA/JAXA mission [12] Benkhoff et al., (2021). ISA has  
118 been developed by the Gruppo di Gravitazione Sperimentale at the Institute for Space Astrophysics  
119 and Planetology (INAF-IAPS) whereas Thales Alenia Space Italy is the manufacturer of both the HAA  
120 and ISA instruments [13] Santoli et al., (2020). ISA data in the BepiColombo mission have been used  
121 so far to better understand the spacecraft dynamics during flybys [14] Magnafico et al.,(2025),[15]  
122 Del Vecchio et al., (2025) and will be used within the orbit determination software to enhance the  
123 reliability of the Mercury Orbiter Radio science Experiment (MORE) results [16] De Filippis et al.,  
124 (2024).

125 The HAA consists of two units: the Accelerometer Control Unit (ACU) and the Accelerometer  
126 Detector Assembly (ADA). The ADA hosts three sensors with their relevant element being a very thin  
127 slat. The sensing mass works as a mechanical harmonic oscillator with a resonance frequency of  
128 about 3.6 Hz. To reduce the down-conversion of out-of-band high-frequency signals, the HAA is  
129 equipped with an out-of-band mechanical noise rejection algorithm. The accelerations are detected  
130 by measuring the movements of the proof mass within the instrument's frame. These movements are  
131 converted into voltage signals by pick-up capacitors. The three sensors, indicated as Acc0, Acc1 and  
132 Acc2, are mounted on mechanical dampers over the electronic module, which contains the Front-  
133 End Electronic (FEE) board. The ACU interfaces with the spacecraft and controls the ADA assembly.



134 The HAA software provides four independent thermal controls, one for each sensor and one for the  
135 FEE. The temperature-controlled point is located on the ADA box. The instrument inflight calibration  
136 is conducted using a couple of control capacitors which are placed under the pick-up capacitors.  
137 These capacitors can be seen as actuators which are able to apply a reference signal to the proof  
138 mass. Table 1 shows the instrument performance indexes declared by the manufacturer after ground  
139 tests.

140  
141

Performance index	Value
Measurement bandwidth	$[10^{-4} - 10^{-1}]$ Hz
Measurement accuracy	$10^{-8}$ m/s <sup>2</sup>
Electronic thermal sensitivity	$10^{-8}$ m/s <sup>2</sup> /°C
Intrinsic thermal sensitivity	$5 \times 10^{-7}$ m/s <sup>2</sup> /°C
Thermal control attenuation factor	700
Intrinsic noise floor	$10^{-9}$ m/s <sup>2</sup> / ÖHz

142 **Table 1** HAA performance indexes

## 143 4 Lunar-Earth gravity assist

144

145 The JUICE mission employs a sequence of gravity assists to increase its energy and adjust its  
146 trajectory for the long journey to the Jovian system. Among these, the Lunar-Earth Gravity Assist  
147 (LEGA), performed in August 2024, represents a novel and highly efficient maneuver. By first  
148 performing a flyby of the Moon with CA at 750 km, followed just few hours later by an Earth flyby (CA  
149 at 6800 km), JUICE exploited the combined gravitational influence of both bodies to achieve a  
150 substantial change in its heliocentric velocity. This dual-body gravity assist allowed to significantly  
151 reduce propellant consumption, enabling the spacecraft to reorient its path toward subsequent  
152 Venus and Earth flybys.

### 153 4.1 HAA operations

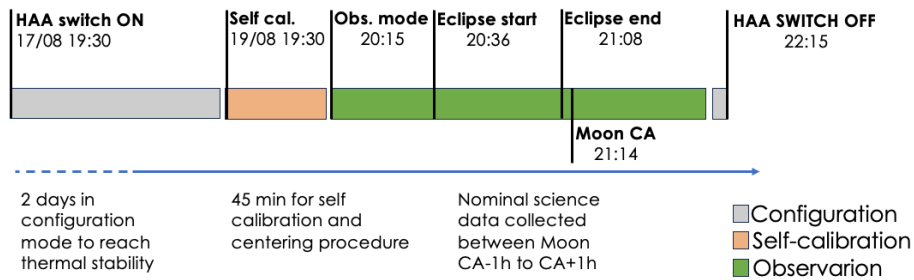
154 The onboard accelerometer was switched ON two days before the lunar gravity assist to ensure the  
155 instrument reached passive thermal stabilization. Although both the sensors and the FEE are  
156 equipped with active thermal control systems, these were not activated during LEGA operations,  
157 because analyses of other in-flight data acquired during earlier instrument checkouts highlighted the  
158 need to still optimize the thermal control settings.

159 The instrument started to collect data ~ 1 hours before Moon CA after a self-calibration and remained  
160 in observation mode till 1 hour after Moon CA. Fig. 1 shows the timeline of HAA operations. In this time  
161 window, different phenomena were expected to produce dynamical effects on the spacecraft, raising  
162 the interest to switch on the instrument.

163



164  
165



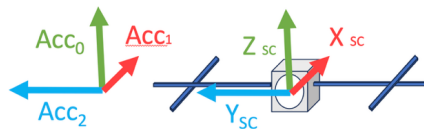
166  
167

**Fig. 1** HAA operations during Lunar gravity assist

168

## 169 4.2 Spacecraft attitude and expected signals

170 An accurate representation of the spacecraft's attitude is essential to reliably model the non-  
 171 conservative forces acting on it. The latest release of the JUICE SPICE kernels [17] Lopez et al. (2023),  
 172 has been used to retrieve the measured attitude of the spacecraft. To describe the orientation of  
 173 JUICE, a body fixed reference frame is used, defined as follows: the  $+\hat{x}_{SC}$  is aligned with HGA  
 174 boresight but points in the opposite direction,  $+\hat{z}_{SC}$  is the spacecraft upper nadir direction where  
 175 some sensitive instruments are mounted on an optical bench, and  $+\hat{y}_{SC}$  axis completes the right-  
 176 handed frame, with  $\pm\hat{y}_{SC}$  hosting the 85 m<sup>2</sup> solar arrays. Fig. 2 shows the relation between each  
 177 accelerometer sensing axis direction and JUICE SPACECRAFT reference frame.



178  
179

**Fig. 2** HAA (left) and JUICE SPACECRAFT (right) reference frames

180

181 During the cruise phase, under nominal attitude conditions, the  $-\hat{x}_{SC}$  direction axis is always oriented  
 182 toward the Sun to shield the spacecraft surfaces from incoming solar heating when JUICE is below  
 183 0.89 AU away from the Sun. Temporary off-pointings ( $\sim 1$  hour) are allowed in between 0.89 and 1.34  
 184 AU, while at greater distance the HGA can point to the Earth. During the lunar flyby, the commanded  
 185 spacecraft attitude was quasi-inertial, meaning that no apparent acceleration was expected to be  
 186 detected by the HAA. Among all the expected signals, the Moon's gravity gradient was the most  
 187 interesting one for calibration purposes and will be described in the next subsection.

188

### 189 4.2.1 Gravity gradient

190 Fig. 3 schematizes the HAA sensing elements as point masses, each associated with a sensing axis  
 191 defined as the direction along which an external acceleration produces the maximum signal. Because  
 192 the centers of gravity of the sensing elements do not coincide with the spacecraft's center of mass,



193 the accelerometer is inherently sensitive to the gravity gradient generated by the Moon's gravitational  
194 field at the sensor locations. The expected signal can be computed using:

195

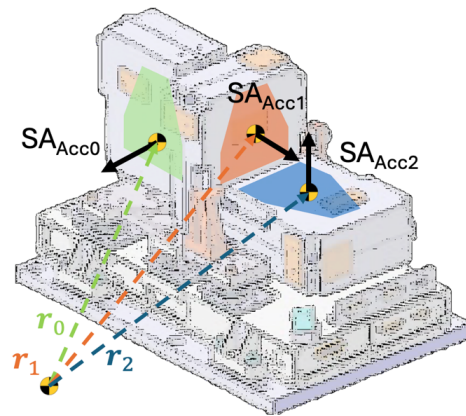
$$\mathbf{a}_{gg}^i = \frac{\mu_m}{|\mathbf{R}_0|^3} (\widehat{\mathbf{R}}_0 \widehat{\mathbf{R}}_0^T - \mathbf{I}_{3 \times 3}) \mathbf{r}_i \quad (1)$$

196

197

198 where  $\mu_m$  is the Moon gravitational parameter,  $\mathbf{R}_0$  is the position vector from JUICE center of mass to  
199 the Moon center of mass, and  $\mathbf{r}_i$  is the position vector from JUICE center of mass to the  $i$ -th HAA  
200 sensing element.

201



202

203

**Fig. 3** HAA sensing element scheme

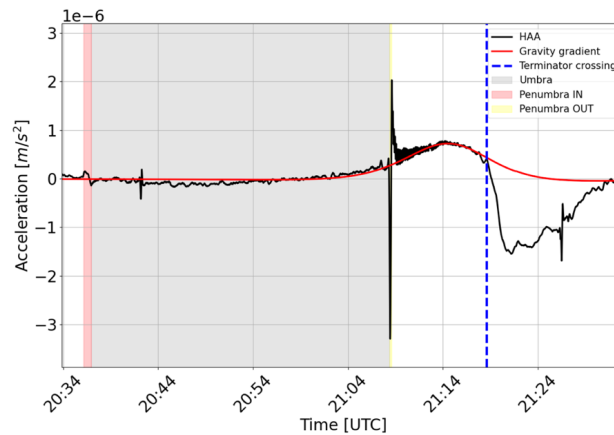
204

205 In this work, only data collected by the Acc0 sensor are presented, as most of the relevant signals  
206 were detected along this axis, which was also the less noisy. Fig. 4 shows the HAA calibrated data  
207 collected by the sensor Acc0 (black curve) compared with the expected gravity gradient signal (red  
208 curve). The HAA measurements show good agreement with the expected signal for most of the time,  
209 but it is evident how the black curve exhibits additional signatures, suggesting the presence of other  
210 perturbing phenomena.

211

212 The grey area corresponds to a solar eclipse experienced by the spacecraft from 20:36 UTC to 21:08  
213 UTC, also visible in the spacecraft ground track in Fig. 5 (blue dots). The abrupt temperature change  
214 in temperature during ingress/egress phases caused thermal snaps that are described in detail in the  
215 next section.

216



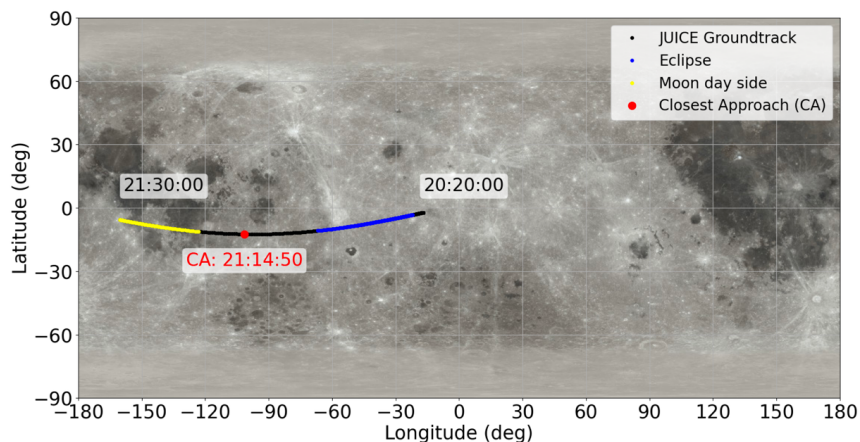
217  
 218

**Fig. 4** HAA calibrated data collected by Acc0 sensor during LEGA

219

#### 220 4.2.2 Thermal snap on solar array

221 Due to the high solar array Sun aspect angle,  $\alpha \approx 70^\circ$ , the expected drop of solar radiation pressure  
 222 acceleration during the eclipse was  $\sim 10^{-8} \text{m/s}^2$ , thus too close to the HAA measurement accuracy to  
 223 be unambiguously detected. Also, the albedo pressure and infrared radiation emitted by the Moon  
 224 were inducing accelerations well below the instrument's sensitivity  $\sim 10^{-9} \text{m/s}^2$ . Instead, the  
 225 sudden absence of solar radiation during the eclipse caused abrupt changes in the spacecraft surface  
 226 temperatures and large thermal gradient between the front and rear surfaces induced thermoelastic  
 227 distortions on the structure.



228  
 229

**Fig. 5** JUICE ground track during Lunar gravity assist

230

231  
 232 This phenomenon, known as thermal snap, can be described mathematically using (2). The resulting  
 233 quasi-static displacements can be expressed in terms of the temperature difference through the



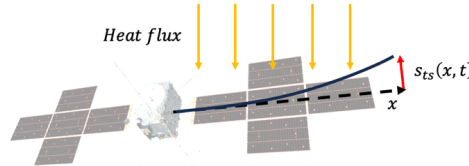
234 thickness of the considered structure [18] Johnston et al. (2000). These displacements are  
 235 proportional to both the surface thermal expansion coefficient  $\alpha_{CTE}$  and the thickness  $h$ . The effect is  
 236 magnified on the spacecraft solar array, due to their large surface area and small thickness, see Fig.  
 237 6. The term  $(1 - \nu^2)$  contains the Poisson's coefficient  $\nu$  and it's used to consider the structural  
 238 response of a wide plate rather than a narrow beam. If the difference between front and back surface  
 239 temperatures  $\Delta T = T_f - T_b$  is not constant in time, the generic point of the solar array, with a distance  
 240  $x$  from the hinge, will be subject to an acceleration  $a_{ts}(t) = \frac{d^2 s_{ts}(t)}{dt^2}$  acting along the solar array normal  
 241 direction  $\hat{n}$ , as described in (3).

242  
 243

$$\vec{s}_{ts}(t)|_x = -\alpha_{CTE}(1 - \nu^2)\Delta T(t) \frac{x^2}{2h} \hat{n} \quad (2)$$

$$\vec{a}_{ts}(t)|_x = \frac{d^2 s_{ts}(t)}{dt^2} = -\alpha_{CTE}(1 - \nu^2) \frac{d^2 \Delta T(t)}{dt^2} \frac{x^2}{2h} \hat{n} \quad (3)$$

244  
 245



246  
 247

**Fig. 6:** JUICE solar array displacement due to thermal snap

248

249 Unfortunately, for the JUICE spacecraft only the solar array back surface temperature  $T_b$  can be  
 250 retrieved from thermistors telemetry, while the front one  $T_f$  is available at a frequency of only one data  
 251 point per month. For this reason, to reconstruct the  $\Delta T$  curve during the eclipse we built a thermal  
 252 mathematical model that describes the heat transmission from front to rear surfaces of the arrays.  
 253 The solar array is modelled as a honeycomb aluminum core surrounded by two aluminum plates that  
 254 exchanges heat via conduction through the core and via radiation from the plates towards internal  
 255 surfaces and to the outer space. The front temperature can be estimated by solving the following  
 256 system of equations [19] J. and S. D. Van der Ha, (2010):

$$\begin{cases} Q_{SUN}/A_p - Q_{APR}/A_p - \sigma_{SB}\epsilon_{SA,f}T_f^4 - \frac{kA_{al}}{h}(T_f - T_b) - \sigma_{SB} \frac{\epsilon_i(1 - A_{al})}{2 - \epsilon_i}(T_f^4 - T_b^4) = C_{p,f} \frac{dT_f}{dt} \\ \sigma_{SB}\epsilon_{SA,f}T_b^4 + \frac{kA_{al}}{h}(T_f - T_b) + \sigma_{SB} \frac{\epsilon_i(1 - A_{al})}{2 - \epsilon_i}(T_f^4 - T_b^4) = C_{p,b} \frac{dT_b}{dt} \end{cases} \quad (4)$$

257 With,

258

259

260

261

262

$$Q_{SUN} = A_p \alpha_{SA} \cos(\alpha(t)) \frac{\phi_{1AU}}{D_s^2} \quad (5)$$



263 Here,  $C_{p,f}$  and  $C_{p,b}$  are the thermal capacity of the front and back surfaces respectively,  $A_p$  is the area  
 264 of the single panel,  $\alpha_{SA}$  is the absorptivity of the panel's front side,  $\varepsilon_{SA,f}$  and  $\varepsilon_{SA,b}$  are the emissivity of  
 265 the panel's front and back sides,  $k$  is the conductivity of the aluminum honeycomb,  $A_{al} = \rho_{hc}/\rho_{al}$  is  
 266 the net aluminum cross section defined as the ratio between the density of the honeycomb and the  
 267 density of the aluminum,  $h$  is the panel's thickness,  $\varepsilon_i$  is the emissivity of the internal surfaces  
 268 (assumed equal to 0.6) and  $\sigma_{SB}$  is the Stephan Boltzmann constant. It has been considered also the  
 269 power extracted from each panel read by the array power regulator  $Q_{APR}$  parameter, obtained from  
 270 telemetry.

271 Model parameters were partly provided by the project ( $k, h, A_p, \varepsilon_{SA,f}, \varepsilon_{SA,b}, \alpha_{SA}$ ) or estimated ( $C_{p,f}, C_{p,b}, \alpha_{CTE}, A_{al}$ )  
 272 by matching the computed rear-side temperature with the corresponding  
 273 measured data, collected in the same reference period. Fig. 7 shows the computed front-side  
 274 temperature (red curve) and rear-side temperature (blue curve), obtained by solving (4, compared  
 275 with the rear measured one (green curve). At this stage, (3 can be applied to compute the thermal  
 276 snap acceleration induced by JUICE's solar array. To compare the modelled acceleration with the  
 277 HAA measurements, the computed acceleration must be projected along the Acc0 sensitive axis and  
 278 scaled by the ratio between the solar array mass and the total spacecraft mass  
 279  $M_{SC} = 5700 \text{ kg}$ . Additionally, the relative displacement between the spacecraft center of mass and  
 280 the solar array center of mass must be considered. Table 2 reports the values of parameters, either  
 281 assumed or estimated, used to model the thermal behavior of JUICE solar arrays.

282

Parameter	Value
$C_{p,f}, C_{p,b}$	800 J/kgK
$A_{al}$	$14 \text{ kg/m}^3$
$h$	23 mm
$k$	117 W/mk
$\varepsilon_{SA,f}, \varepsilon_{SA,b}$	0.82, 0.79
$\alpha_{SA}$	0.80
$\varepsilon_i$	0.6
$\alpha_{CTE}$	$3.5 \times 10^{-6} \text{ K/m}$
$A_p$	8.8 m <sup>2</sup>

283

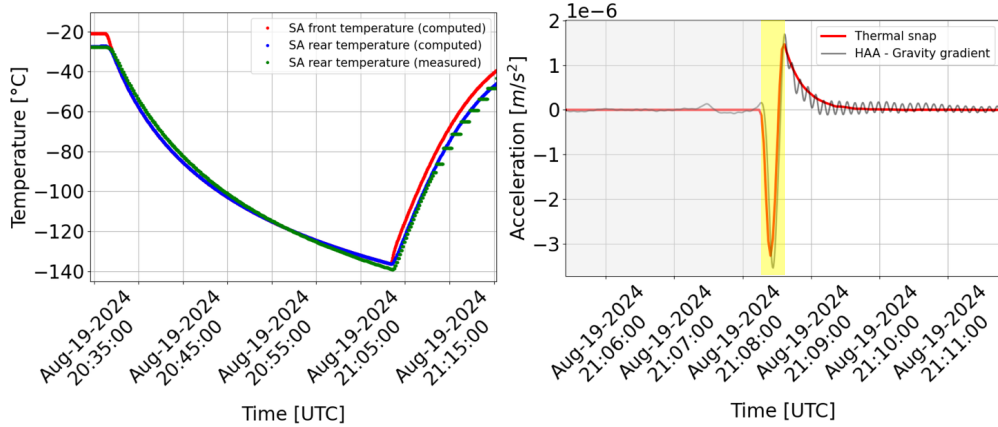
**Table 2** JUICE solar array properties

284 Fig. 8 shows the comparison between HAA Acc0 calibrated data after the removal of the Moon's  
 285 gravity gradient signal and the expected thermal snap acceleration. This latter primarily occurred  
 286 during the penumbra phase (yellow shadowed area), where the rapid transition from umbra condition  
 287 (grey shadowed area) to the illuminated condition (white area), amplified both the thermal gradient  
 288 and its second derivative. The computed quasi-static displacement of the solar array tip was  
 289 estimated to be approximately 50 mm, corresponding to  $\sim 0.3 \text{ deg}$  of angular displacement. After the  
 290 penumbra phase, HAA data shows a clear periodic signal easily explained by thermally induced  
 291 vibrations of the solar array structure. This is confirmed by the amplitude spectral density (ASD)  
 292 computed on HAA data after the spacecraft came back in full illumination (white area in Fig. 8), where  
 293 we found that the dominant frequency closely matches the first out-of-plane mode of the solar array,  
 294 as shown in Fig. 9. A similar phenomenon was observed at penumbra ingress; however, due to the



295 slower transition from illumination to umbra, the perturbing signal was weaker, and the resulting  
 296 displacement and corresponding acceleration detected by HAA were correspondingly smaller.

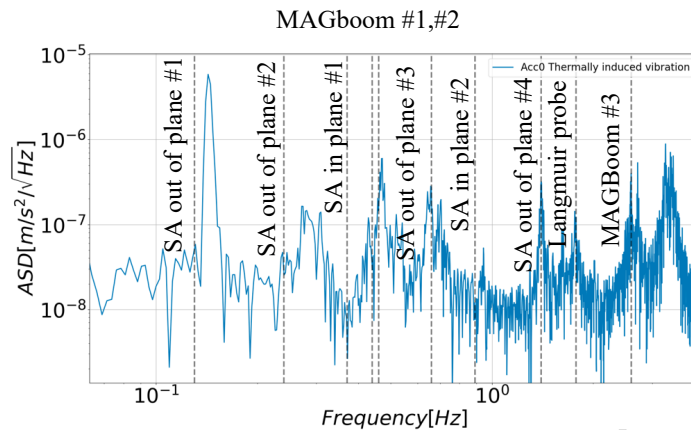
297



298  
 299

**Fig. 7** Estimated solar array surface temperature on the front side (red) and rear side (blue), compared with measured rear-side temperature (green).

**Fig. 8** HAA calibrated data collected during umbra exit (black curve) and computed thermal snap acceleration (red).



300

301

**Fig. 9** ASD computed on HAA data soon after exit penumbra phase

302

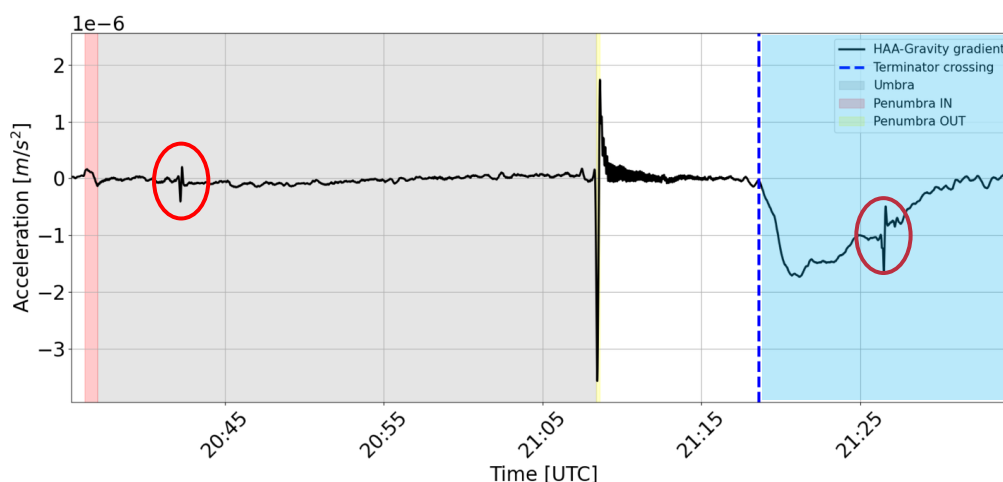
### 303 4.3 Unexpected signals

304 The great added value of a HAA onboard the spacecraft lies not only in its ability to directly measure  
 305 expected accelerations that are difficult to model, but also in its capability to detect unforeseen  
 306 accelerations which, if left uncalibrated, could degrade the performance of scientific experiments.  
 307 During LEGA Moon flyby, HAA data revealed several unexpected signatures. These were already  
 308 visible in previous pictures but left voluntarily uncommented. Fig. 10 puts evidence now on two similar



309 signals about  $\sim 10^{-4} m/s^2$  detected at 20:42 UTC and 21:26 UTC, highlighted within the red circles,  
310 while another significant acceleration of  $\sim 2 \cdot 10^{-6} m/s^2$  was detected shortly after the spacecraft  
311 crossed the lunar terminator (indicated by the blue dotted line and blue shaded area thereafter).

312



313  
314

**Fig. 10** HAA Acc0 calibrated data

315

#### 316 4.3.1 Submillimetre Wave Instrument operations

317 The first signal, identified by red circles in the Fig. above, appears to be associated with spacecraft  
318 activity related to the Submillimeter Wave Instrument (SWI), the only one featuring a steerable  
319 component and active at the corresponding epochs: a telescope mounted on the same spacecraft  
320 plate as the HAA (+X vault). Personal communication with the SWI instrument team confirmed that  
321 at 20:41:58 UTC the telescope was rotated by 72 degrees in the along-track direction to point toward  
322 the Moon (nadir position). A second rotation, in the opposite direction by 54 degrees, was performed  
323 at 21:27 UTC to observe the Moon in a backward-looking configuration. These mechanical operations  
324 primarily excited resonance mode of the spacecraft's MAGboom structure (0.44, 0.46, 2.6 Hz) and  
325 solar arrays (0.13, 0.21, 0.89 Hz). The influence of these events on HAA data capability to support 3GM  
326 experiment has yet to be fully assessed. It is likely that dedicated tests will be required to thoroughly  
327 characterize possible interference issues.

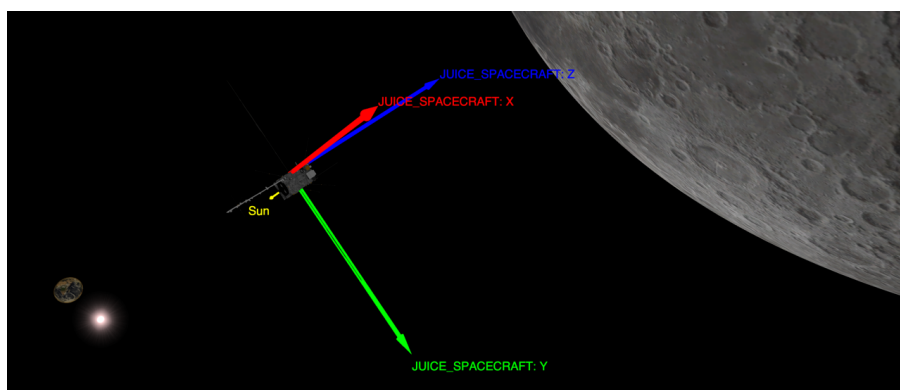
#### 328 4.3.2 Outgassing event

329 The second SWI event is superimposed to another clearly visible low-frequency phenomenon  
330 occurred onboard the JUICE spacecraft. After the eclipse event, JUICE reached the Moon CA at  
331 21:14:50 UTC and soon after crossed the terminator at 21:18:35 UTC. Fig. 11 shows JUICE attitude  
332 during the terminator crossing. At that moment, the +Z and +X directions of JUICE were oriented  
333 toward the illuminated surface of the Moon, receiving most of the incoming heat due to lunar albedo  
334 and infrared radiation. One of the most plausible explanations for the effect is that the multilayer  
335 insulation (MLI) on the +Z vault may have accumulated frozen contaminants during the early cruise  
336 phase, as this surface is typically exposed to deep space. Given the combination of high incoming



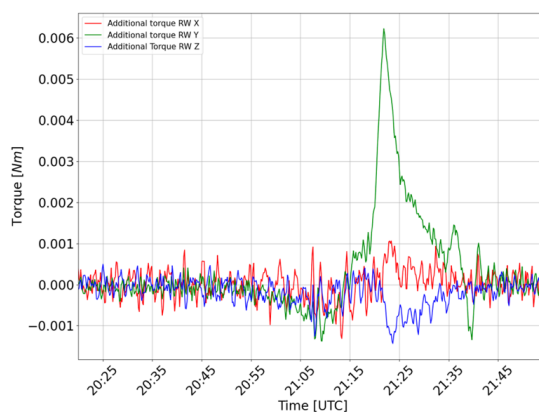
337 radiation and the low thermal inertia of the MLI, it is likely that its temperature increased rapidly,  
338 potentially triggering an outgassing event. A similar phenomenon was observed on the BepiColombo  
339 ESA–JAXA mission during a Venus swing-by [20] De Filippis et al., (2025).

340  
341



342  
343  
344  
345  
346

**Fig. 11** JUICE attitude at terminator crossing (21:18 UTC) from Cosmographia



347  
348  
349  
350  
351

**Fig. 12** Additional torques exerted by reaction wheels on the spacecraft

352 The JUICE spacecraft attitude and orbit control system (AOCS) also detected this event. Fig. 12  
353 shows the unmodelled torque generated by the reaction wheels to maintain the commanded quasi-  
354 inertial attitude. The dominant torque component was observed along the +Y JUICE SPACECRAFT  
355 axis, while the main acceleration measured by HAA was along the -Z JUICE SPACECRAFT axis.  
356 Assuming that  $M = M_{SC} r \times a$ , where  $M$  is the unmodelled torque generated by the reaction wheels,  
357  $r$  is the vector distance from the spacecraft center of mass and the outgassing location and  $a$  is the  
358 unmodelled acceleration measured by HAA, adopting the reasonable simplification that both torque



359 and force acted predominantly along a single axis, the outgassing appears to have occurred  
360 approximately 50 cm from the spacecraft's center of mass, in the -X JUICE SPACECRAFT direction.

361 To further investigate the impact of the suspected outgassing event, we conducted an orbit  
362 determination analysis using Doppler data, collected during the Lunar gravity assist. The radiometric  
363 dataset consisted of X band two-way coherent Doppler data acquired by the ESTRACK ground  
364 stations at:

- 365 • New Norcia on 2024-08-19, from 11:09 UTC to 22:10 UTC, with an observed Doppler noise  
366 level of 0.035 mm/s @60s, and
- 367 • Cebreros, from 2024-08-19 22:26 UTC to 2024-08-20 04:15 UTC, with an observed Doppler  
368 noise level of 0.046 mm/s @60s.

369 Note that no 3GM's KaT operations were possible as it would have required a Ka band uplink signal,  
370 currently only available at Malargüe ground station. This analysis was performed with ESA's GODOT  
371 software, using a setup adapted from radio science analyses [21] Cappuccio *et al.*, (2025). In a first  
372 attempt we tried to solve for  $\Delta V_i$  components along all three spacecraft axes X, Y and Z, and the time  
373 event, but the reduced radio metric data set available for this analysis was not sufficient to fully  
374 decorrelate the three estimated impulses, resulting in a too high covariance matrix that was both  
375 consistent with estimates carried out by the Flight Dynamics team [22] Syndercombe *et al.* (2025)  
376 and null  $\Delta V_i$ . The estimated time of the outgassing event was 2024-08-19 21:26 ± 42 seconds UTC.  
377 We had to accept to carry out a second constrained analysis in which  $\Delta V_y$  was kept null and we  
378 obtained a better statistical compatibility with FD solution. In summary, the analysis based on  
379 radiometric data alone provide only limited constraints on the characteristics of the outgassing event  
380 which is detected with much greater sensitivity by accelerometer data. Indeed, along the +Z direction,  
381 HAA measurements are consistent with a DV=-0.7mm/s. Integrating a different portion of HAA data  
382 where no signals were detected, we associated to the outgassing impulse a maximum error of 0.1  
383 mm/s. Along the +X direction, HAA measurements are strongly affected by the thermal disturbances,  
384 making the collected data unreliable.

385 After the outgassing, the spacecraft's momentum changed according to the push exerted by  
386 sublimated products. Using the conservation of momentum, the sublimated product's effective exit  
387 velocity  $V_{sub}$  and its mass  $m_{sub}$  can be related to the overall change in the spacecraft's velocity  $DV$ :

388

$$m_{sub}V_{sub} = M_{SC}DV \quad (6)$$

389

390 The most plausible outgassing product is water ice, as also suggested by observations from different  
391 instrument teams during the flyby. Under this assumption, the effective exit velocity of the sublimated  
392 water vapor can be estimated by considering the theoretical maximum velocity for a sublimating gas,  
393 given by:

394

$$V_{lim} = \sqrt{\frac{2\gamma RT}{\gamma - 1}} \quad (7)$$



395 where  $\gamma$  is the ratio of specific heat of water,  $R$  is the specific gas constant, and  $T$  is the total  
396 temperature at zero velocity. For typical value of  $\gamma = 1.33$  and  $T = 300K$ , the  $V_{lim} = 1000 m/s$  [23]  
397 Sandford *et al.*,(2020). However, this is only a physical maximum value, and the true value of the  
398 effective exit velocity is not easy to retrieve. Considering a  $V_{sub} = 1/2V_{lim} = 500 m/s$ , it's possible  
399 to give an estimate of the order of magnitude of the sublimated product's mass:

400  
401

$$m_{sub} = M_{SC}DV/V_{sub} = 8g \quad (8)$$

402 Note that the true value of the effective exit velocity may differ in relation to the sublimation dynamics.  
403 If  $V_{sub} = V_{lim} = 1000 m/s$ , the outgassed mass became  $m_{sub} = 4 g$ . Moreover, the estimation of  
404 sublimated particles along the other spacecraft axes is even more challenging. However, the  
405 accelerometer data provided indication that the outgassing components along those directions are  
406 significantly smaller than along the +Z JUICE SPACECRAFT axis.

## 407 5 Conclusions

408 This work presents a comprehensive analysis of data collected by the High Accuracy Accelerometer  
409 instrument during the JUICE LEGA flyby at the Moon. The calibrated scientific dataset was compared  
410 with predicted non-gravitational signals derived from analytical models, showing good agreement  
411 between the HAA Acc0 sensor measurements and the expected reference signals. In details, the HAA  
412 on board JUICE detected the effect of the Moon gravity gradient on its sensible masses as well as  
413 thermoelastic displacement of solar array during the penumbra phases. In addition, unexpected  
414 dynamical effects on the spacecraft have been detected. The operations activities of the  
415 Submillimetre Wave Instrument (SWI) were clearly visible in the HAA data. The rotation of the  
416 instrument's steerable telescope, performed before and after the Moon closest approach to achieve  
417 nadir pointing, excited structural resonance modes of the spacecraft, notably the MAGboom and  
418 solar array. The resulting vibrations were observed on all three HAA axes. Furthermore, an outgassing  
419 event occurred soon after the spacecraft transition over the Moon terminator was detected by the  
420 instrument Acc0 channel. The source of the signal was also confirmed by multi-instrument analysis  
421 and spacecraft AOCS telemetry. The measured accelerations profile suggested that the outgassing  
422 happened mostly along spacecraft -Z direction producing a total  $DV = 0.7 mm/s$  along the same  
423 direction. The estimated order of magnitude for the mass of sublimated water ice product was around  
424 8 g. These observations provided important information for the instrument calibration and spacecraft  
425 dynamic environment during close flyby. The acquisition of HAA in-flight data prior the start of the  
426 scientific phase will be fundamental to achieve optimal instrument performance. It will enable the  
427 definition of the most suitable instrument configuration parameters, enhancing the reliability of  
428 subsequent measurements, and supporting the development of improved operational strategies.  
429 Early data will help optimize the coordination with other onboard instruments, thereby maximizing the  
430 overall scientific return of the mission.



## 431 6 Data availability

432

433 All raw data can be provided by the corresponding authors upon request

## 434 7 Author contribution

435

436 UDF,PC,MDB wrote the manuscript draft; UDF,MDB,LI planned the operations; UDF,PC analyzed  
437 the data; UDF,PC,MDB,IDS,DD,LI reviewed and edited the manuscript.

438

## 439 8 Competing interests

440

441 The authors declare that they have no conflict of interest.

## 442 9 Acknowledgments

443 The authors are grateful to the Italian Space Agency (ASI) for financial support through ASI-INAF  
444 Agreement No. 2023-6-HH.0 in the context of ESA's JUICE mission.

445

## 446 10 References

447

- 448 [1] O. Grasset *et al.*, “Jupiter ICy moons Explorer (JUICE): An ESA mission to orbit Ganymede  
449 and to characterise the Jupiter system,” *Planet Space Sci*, vol. 78, pp. 1–21, 2013, doi:  
450 <https://doi.org/10.1016/j.pss.2012.12.002>.
- 451 [2] O. Grasset, D. Titov, and O. Witasse, “Jupiter Icy Moon Explorer Mission,” in *Encyclopedia of*  
452 *Astrobiology*, M. Gargaud, W. M. Irvine, R. Amils, P. Claeys, H. J. Cleaves, M. Gerin, D. Rouan,  
453 T. Spohn, S. Tirard, and M. Viso, Eds., Berlin, Heidelberg: Springer Berlin Heidelberg, 2023, pp.  
454 1587–1591. doi: 10.1007/978-3-662-65093-6\_5283.
- 455 [3] U. De Filippis *et al.*, “Monitoring JUICE deployment operations with high-accuracy  
456 accelerometer data,” *Acta Astronaut*, vol. 225, pp. 719–728, Dec. 2024, doi:  
457 [10.1016/j.actaastro.2024.09.047](https://doi.org/10.1016/j.actaastro.2024.09.047).
- 458 [4] P. Cappuccio, M. Di Benedetto, G. Cascioli, and L. Iess, “Report on JUICE 3GM gravity  
459 experiment performance,” in *European Planetary Science Congress*, 2018, pp. EPSC2018-  
460 1066.
- 461 [5] P. Cappuccio *et al.*, “Report on First Inflight Data of BepiColombo’s Mercury Orbiter Radio  
462 Science Experiment,” *IEEE Trans Aerosp Electron Syst*, vol. 56, no. 6, pp. 4984–4988, Dec.  
463 2020, doi: 10.1109/TAES.2020.3008577.
- 464 [6] A. Shapira *et al.*, “An Ultra Stable Oscillator for the 3GM experiment of the JUICE mission,” in  
465 *2016 European Frequency and Time Forum (EFTF)*, IEEE, Apr. 2016, pp. 1–5. doi:  
466 [10.1109/EFTF.2016.7477766](https://doi.org/10.1109/EFTF.2016.7477766).
- 467 [7] P. Cappuccio, M. Di Benedetto, D. Durante, and L. Iess, “Callisto and Europa Gravity  
468 Measurements from JUICE 3GM Experiment Simulation,” *Planet Sci J*, vol. 3, no. 8, p. 199,  
469 Aug. 2022, doi: 10.3847/PSJ/ac83c4.



- 470 [8] P. Cappuccio *et al.*, “Ganymede’s gravity, tides and rotational state from JUICE’s 3GM  
471 experiment simulation,” *Planet Space Sci*, vol. 187, p. 104902, 2020, doi:  
472 <https://doi.org/10.1016/j.pss.2020.104902>.
- 473 [9] F. De Marchi, P. Cappuccio, G. Mitri, and L. Iess, “Frequency-dependent Ganymede’s tidal  
474 Love number k2 detection by JUICE’s 3GM experiment and implications for the subsurface  
475 ocean thickness,” *Icarus*, vol. 386, p. 115150, 2022, doi:  
476 <https://doi.org/10.1016/j.icarus.2022.115150>.
- 477 [10] I. di Stefano, P. Cappuccio, M. Di Benedetto, and L. Iess, “A test of general relativity with  
478 ESA’s JUICE mission,” *Advances in Space Research*, vol. 70, no. 3, pp. 854–862, Aug. 2022,  
479 doi: 10.1016/j.asr.2022.05.005.
- 480 [11] P. Cappuccio and G. Cascioli, *ESA’s JUICE End-to-End Orbit Determination Simulation to  
481 Calibrate On-Board Accelerometer*. 2018.
- 482 [12] J. Benkhoff *et al.*, “BepiColombo - Mission Overview and Science Goals,” *Space Sci Rev*, vol.  
483 217, no. 8, p. 90, 2021, doi: 10.1007/s11214-021-00861-4.
- 484 [13] F. Santoli *et al.*, “ISA, a High Sensitivity Accelerometer in the Interplanetary Space,” *Space Sci  
485 Rev*, vol. 216, no. 8, p. 145, 2020, doi: 10.1007/s11214-020-00768-6.
- 486 [14] C. Magnafico *et al.*, “Italian Spring Accelerometer measurements of unexpected Non  
487 Gravitational Perturbation during BepiColombo second Venus swing-by,” *Acta Astronaut*, vol.  
488 232, pp. 14–22, Jul. 2025, doi: 10.1016/j.actaastro.2025.02.037.
- 489 [15] E. Del Vecchio *et al.*, “First Analysis of BepiColombo Radio Science and Accelerometer Data  
490 Acquired During Venus and Mercury Flybys,” *IEEE Trans Aerosp Electron Syst*, vol. 60, no. 4,  
491 pp. 5604–5612, Aug. 2024, doi: 10.1109/TAES.2024.3381582.
- 492 [16] U. De Filippis *et al.*, “Pseudo-Drag-Free System Simulation for Bepicolombo Radio Science  
493 Using Accelerometer Data,” *Journal of Guidance, Control, and Dynamics*, vol. 47, no. 4, pp.  
494 685–696, Jan. 2024, doi: 10.2514/1.G007916.
- 495 [17] Lopez, A. E., Valles, R., Andres, R., & Arviset, C. (2023). An Update on SPICE for ESA  
496 Missions. *Bulletin of the AAS*, 55(8). <https://baas.aas.org/pub/2023n8i109p08>
- 497 [18] J. D. Johnston and E. A. Thornton, “Thermally Induced Dynamics of Satellite Solar Panels,” *J  
498 Spacecr Rockets*, vol. 37, no. 5, pp. 604–613, Sep. 2000, doi: 10.2514/2.3633.
- 499 [19] J. and S. D. Van der Ha, “Thermal Radiation Effects on Deep-Space Trajectories,” *Advances in  
500 the Astronautical Sciences*, vol. 136, pp. 1861–1880, Jan. 2010.
- 501 [20] U. De Filippis, C. Lefevre, M. Lucente, C. Magnafico, and F. Santoli, “Characterization of the  
502 outgassing event during BepiColombo second Venus flyby using Italian Spring Accelerometer  
503 data,” *Acta Astronaut*, vol. 226, pp. 11–19, Jan. 2025, doi: 10.1016/j.actaastro.2024.09.062.
- 504 [21] P. Cappuccio *et al.*, “Analysis of Radio Science Data from the KaT Instrument of the 3GM  
505 Experiment During JUICE’s Early Cruise Phase,” *Aerospace*, vol. 12, no. 1, p. 56, Jan. 2025,  
506 doi: 10.3390/aerospace12010056.
- 507 [22] T. Syndercombe, F. Budnik, and R. Meles, “The JUICE navigation campaign for the first  
508 combined Lunar-Earth gravity assist,” in *18th International Conference on Space Operations*,  
509 Montreal: SpaceOps-2025, May 2025.
- 510 [23] S. A. Sandford *et al.*, “Outgassing from the OSIRIS-REx sample return capsule:  
511 characterization and mitigation,” *Acta Astronaut*, vol. 166, pp. 391–399, Jan. 2020, doi:  
512 10.1016/j.actaastro.2019.07.043.
- 513